

1 **Higher viral virulence accelerates the evolution of host resistance**

2

3

4 Carolin C. Wendling^{1,2*}, Janina Lange¹, Heiko Liesegang³, Michael Sieber⁴, Anja
5 Pöhlein³, Boyke Bunk⁵, Jelena Rajkov^{1,6}, Henry Goehlich¹, Olivia Roth^{1,6†}, Michael A.
6 Brockhurst^{7†}

7

8

9 ¹GEOMAR Helmholtz Centre for Ocean Research Kiel, Marine Evolutionary Ecology, Düsternbrooker
10 Weg 20, 24105 Kiel, Germany

11

12 ²ETH Zürich, Institute of Integrative Biology, Universitätstrasse 16, CHN D 33, 8092 Zürich,
13 Switzerland

14

15 ³Georg-August-University Göttingen, department of genomic and applied microbiology, Grisebachstr 8
16 37077 Göttingen, Germany.

17

18 ⁴Max Planck Institute for Evolutionary Biology, August-Thienemann-Str. 2, 24306 Plön, Germany

19

20 ⁵Leibniz Institute DSMZ-German Collection of Microorganisms and Cell Cultures, Department
21 Bioinformatics and Databases, Inhoffenstr. 7B, 38114 Braunschweig, Germany

22

23 ⁶Kiel University, Marine Evolutionary Biology, Am Botanischen Garten 1-9, 24118 Kiel, Germany

24

25 ⁷Division of Evolution and Genomic Sciences, University of Manchester, Dover Street, Manchester M13
26 9PT, UK

27

28

29 *Corresponding author:

30 E-mail: carolin.wendling@env.ethz.ch; Phone: +41 44 633 80 26

31

32 † shared last author

33 **Abstract**

34 Parasites and pathogens vary strikingly in their virulence and the resulting selection
35 they impose on their hosts. While the evolution of different virulence levels is well
36 studied, the evolution of host resistance in response to different virulence levels is less
37 understood and as of now mainly based on theoretical predictions. Increased virulence
38 can increase selection for host resistance evolution if resistance costs are outweighed
39 by the benefits of avoiding infection. To test this, we experimentally evolved the
40 bacterium *Vibrio alginolyticus* against two variants of the filamentous phage,
41 VALGΦ8, that differ in their virulence. The bacterial host exhibited two alternative
42 defence strategies against future viral infection: (1) super infection exclusion (SIE)
43 whereby viral-infected cells were immune to subsequent infection at a cost of reduced
44 growth, and (2) surface receptor mutations in genes encoding the MSHA type-IV pilus
45 providing resistance to infection by preventing viral binding. While SIE emerged
46 rapidly against both viruses, resistance evolved faster against the high virulence
47 compared to the low virulence virus. Using a mathematical model of our system we
48 show that increasing virulence strengthens selection for resistance due to the higher
49 costs of infection suffered by SIE immune hosts. In both the experiments and the model,
50 higher levels of evolved resistance in the host population drove more rapid virus
51 extinction. Thus, by accelerating the evolution of host resistance, more virulent viruses
52 caused shorter epidemics.

53

54 **Keywords:** virus, virulence, filamentous phages, experimental evolution, resistance
55 evolution

56 INTRODUCTION

57 Infectious organisms vary strikingly in their level of virulence and the resulting
58 selection they impose on hosts. Indeed, even closely related viruses, such as different
59 strains of myxoma (1) or corona viruses (2), can differ greatly in virulence. While the
60 evolution of virulence has been studied extensively during the last two decades, both
61 using selection experiments (3-5) and observations of parasites evolved in nature (6, 7),
62 how hosts respond to virulence-mediated selection is less well-explored. How virulence
63 will impact evolutionary trajectories of resistance in a host population, and how these
64 trajectories change with different levels of virulence, has been subjected to theoretical
65 investigation. In general, increased virulence strengthens selection for the evolution of
66 host resistance if the costs of resistance are outweighed by the benefits of avoiding
67 infection (8-10). As such, at very low virulence, although infection is common, resistance
68 is not favoured because the cost of resistance is likely to exceed any benefits of avoiding
69 mild disease (9). With increasing virulence, resistance is more strongly selected as the
70 cost of resistance becomes outweighed by the detrimental effects of more severe disease,
71 leading to the more rapid evolution of resistance (10). However, at extremely levels of
72 high virulence, selection for resistance can weaken once more, due to declining infection
73 prevalence (8). Experimental tests of these predictions are, however, lacking.

74 To explore how viral virulence influences the dynamics of host resistance evolution,
75 we designed a selection experiment using the model bacterium *Vibrio alginolyticus*
76 K01M1 as a host and two variants of the filamentous phage, VALGΦ8, that differ in their
77 virulence but are otherwise isogenic (Table 1). Filamentous phages (family *Inoviridae*)—
78 i.e., long, thin proteinaceous filaments which contain a circular single-stranded DNA
79 genome—have been shown to be ideal model systems to study virulence evolution (3, 5).
80 Filamentous phages establish chronic infections whereby virions are continuously

81 released without lysis. Although filamentous phages do not kill their host, infections
82 cause harm by reducing host growth rates. This is because the host cell pays the metabolic
83 costs resulting from phage replication and from phage-encoded proteins inserted into the
84 bacterial membrane (11). Thus, virulence here is defined as the reduction in bacterial
85 growth resulting from phage infection, which can be directly quantified by measuring the
86 reduction in bacterial growth rate caused by phage infection relative to the growth rate of
87 phage-free cultures.

88 During chronic infections, most phage genes are repressed to ensure host cell
89 viability (12). This is achieved through the action of prophage encoded repressor proteins
90 whose actions also prevent superinfection (i.e., superinfection exclusion, SIE) by the
91 same (or closely related (13)) phage(s). In the case of filamentous phages, SIE immunity
92 is provided through the production of the phage-encoded receptor-binding protein pIII
93 which blocks primary and secondary phage receptors (11). Alternatively, it is possible for
94 bacteria to acquire resistance to filamentous phage infection through mutations causing
95 alterations to the surface receptors that the phages bind to, thus preventing phage infection
96 (15).

97 Combining experimental evolution with whole genome sequencing, we show that
98 SIE immunity arose rapidly and at a similar rate against both phages, whereas resistance
99 evolved more rapidly against the high compared to the low virulence phage, driving faster
100 extinction of the high virulence phage. Using an experimentally parameterised
101 mathematical model we show that accelerated replacement of SIE immunity by resistance
102 was driven by increasing costs of infection, in terms of reduced growth, suffered by SIE
103 immune hosts with increasing viral virulence. Resistance mutations were identified in
104 genes encoding the MSHA type IV pilus, which pleiotropically caused reduced motility
105 of these resistant bacteria. Together these data show that higher viral virulence accelerated

106 the evolution of resistance, which consequently drove faster virus extinctions and shorter
107 viral epidemics.

108 **RESULTS AND DISCUSSION**

109 **Ecological dynamics vary according to phage virulence**

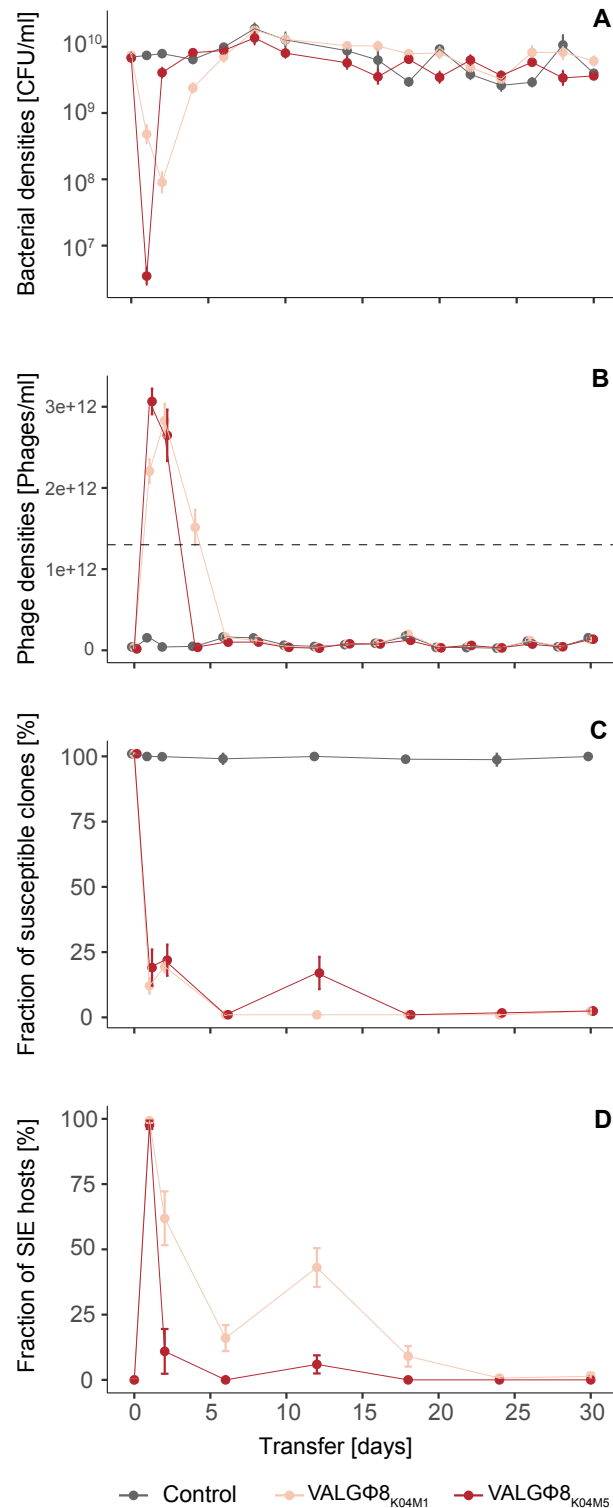
110 To explore how variation in virulence influences the dynamics of host resistance
111 evolution, we experimentally evolved the bacterium *Vibrio alginolyticus* K01M1 with or
112 without one of two isogenic filamentous phages that differ in their virulence—
113 VALGΦ8_{K04M5} which reduces bacterial growth by 73% (higher virulence) or
114 VALGΦ8_{K04M1} which reduces bacterial growth by 58% (lower virulence, Table 1)—for
115 30 serial transfers (~240 bacterial generations). We first compared the ecological
116 dynamics of bacterial and phage populations between treatments. Phages reduced
117 bacterial densities by several orders of magnitude in both phage treatments compared to
118 no phage control populations (Figure 1a). The immediate reduction (measured 24 hours
119 post infection [hpi]) in bacterial density was greater in populations exposed to the higher
120 virulence phage (VALGΦ8_{K04M5}) than the lower virulence phage (VALGΦ8_{K04M1}; Figure
121 1a). Correspondingly, in both treatments, phages amplified massively and rapidly,
122 reaching 3.01×10^{12} PFU/ml (VALGΦ8_{K04M5}) 24 hpi and 2.83×10^{12} PFU/ml
123 (VALGΦ8_{K04M1}) 48 hpi (Figure 1b), before declining to levels comparable to control
124 populations (note that the genome of *V. alginolyticus* K01M1 contains a resident phage,
125 VALGΦ6, that produces phage particles at a low background rate). These data suggest
126 that the strong reduction in bacterial densities at the beginning of the experiment (Figure
127 1a) directly resulted from the costly production of viral particles (Figure 1b). Over time,
128 however, the densities of bacterial populations exposed to the higher virulence phage
129 recovered three times faster than populations exposed to the lower virulence phage
130 (significant phage:transfer interaction in gls-model: $F_{15,186}=6.58$, $p<0.001$, Figure 1a).
131 Bacterial population recovery was accompanied by declining phage densities in both
132 treatments, but phage survival varied according to phage virulence (log-rank test:

133 $\text{Chisq}_1=4.9, p=0.03$), with the higher virulence phage going extinct more rapidly than the
134 lower virulence phage (Figure 4a).

135

136 **Rapid emergence of superinfection exclusion immunity**

137 These bacteria-phage population dynamics suggest that the emergence of bacterial
138 defences against phage infection may have enabled recovery of the host population.
139 Consistent with this hypothesis, the proportion of susceptible hosts rapidly declined to
140 zero within 24 hours in both treatments and remained so for the duration of the experiment
141 (Figure 1c). Bacteria can develop protection from filamentous phage infection by two
142 distinct mechanisms: superinfection exclusion (SIE) immunity, where already infected
143 cells are protected from subsequent infection by the same phage through phage-encoded
144 genes (14), or resistance, for instance via modification of the bacterial phage receptor,
145 preventing phage from entering the host cell (15). To quantify the frequency of SIE
146 immunity we used PCR with primers that target specifically VALG Φ 8 to test for the
147 presence of the relevant phage in the bacterial genome (the presence of a PCR product
148 suggests SIE due to the presence of VALG Φ 8 and those clones are from here on denoted
149 as Φ -carriers). SIE rapidly increased in frequency and dominated bacterial populations in
150 both treatments after 24 hours (Figure 1d). However, after 48 hours, the proportion of SIE
151 hosts began to decline, and did so significantly faster in populations that had been exposed
152 to the higher virulence phage (Figure 1d, significant phage:transfer interaction in glm:
153 $F_{6,60}=10.18, p<0.001$). Given that these populations contained no susceptible bacteria
154 from 24 hours onwards (out of 24 tested colonies per timepoint), the subsequent decline
155 of SIE hosts suggests their displacement by the invasion of resistant genotypes, and that
156 this was more strongly selected for by the higher virulence phage.



157

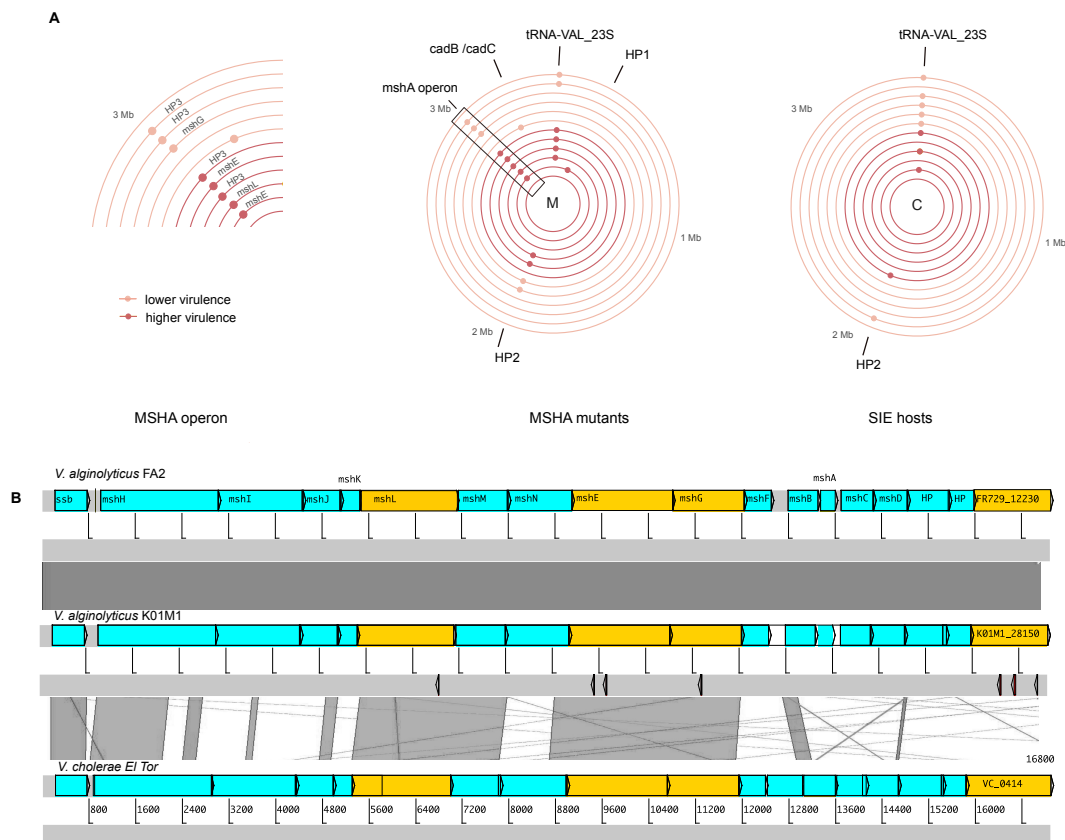
158 **Figure 1 Population dynamics over 30 transfers.** (A) Bacteria in CFU/ml, (B) Phages in PFU/ml, the
 159 grey dashed line represents the quantification limit below which quantifying filamentous phages using
 160 spectrophotometry is inaccurate, note: free phages in the control treatment stem from the low-replicating
 161 resident phage VALGΦ6 (see Table 1) (c) Fraction of susceptible clones (n=24), and (d) Fraction of SIE
 162 hosts within phage-resistant clones. Fractions are based on 24 random clones per replicate population per
 163 timepoint. In all panels, data are represented as mean of six replicate populations per treatments, error bars
 164 represent standard errors. Colours correspond to one of three experimental treatments, lower virulence
 165 VALGΦ8_{K04M1} (light red), higher virulence VALGΦ8_{K04M5} (dark red), no phage (grey).

166 **Resistance is associated with mutations in MSHA type IV pilus encoding genes**

167 To test if the decline of SIE hosts after 24 hours was driven by the invasion of surface
168 receptor modification resistance, we used whole genome sequencing (WGS) of two
169 randomly chosen clones from each population isolated at transfer 2: one PCR-positive
170 clone (Φ -carrier; resistance through superinfection exclusion) and one PCR-negative
171 clone (resistant but not phage carrying) to identify mutations. We observed no loci with
172 mutations on chromosome 2 or the plasmid pI9064, but on chromosome 1 we identified
173 12 loci with mutations that were not present in clones from the control treatment,
174 suggesting that these were associated with phage-mediated selection. Of these 12 loci,
175 three were randomly distributed across PCR-positive and PCR-negative clones. This
176 included an intergenic region between tRNA-Val and the 23S ribosomal RNA, that has
177 been repeatedly hit in both clone-types and phage-treatments, but whose function we
178 cannot explain. The remaining nine loci were exclusive to PCR-negative clones
179 suggesting a potential role in evolved phage resistance. Of these nine loci, eight had
180 substitutions, duplications, insertions, or deletions in four different genes belonging to the
181 MSHA type IV pilus operon (*mshL*, *mshE*, *mshG*, *K01M1_28150*; Figure 2a/ Table S1).
182 Among those, three caused severe frameshift mutations that presumably have a high
183 impact on the function of these proteins. While one locus (*K01M1_28150*) was affected
184 twice in both phage treatments, all other loci were treatment specific with mutations in
185 *mshL* and *mshE* being exclusively found against the higher virulence phage and in *mshG*
186 against the lower virulence phage. Moreover, we found more mutated MSHA-loci among
187 clones exposed to the higher virulence (5/6) compared to the lower virulence phage (3/6).
188 This supports our previous findings, which suggested a stronger selection for resistance
189 against the higher virulence virus.

190 The absence of mutated MSHA-loci in PCR positive clones paired with a high
191 prevalence in PCR-negative clones (8/12) suggests strongly parallel evolution of phage
192 resistance. The MSHA operon is highly conserved across *Vibrio* clades (Figure 2b), and
193 we found one corresponding ortholog to each gene in the *V. cholerae* El Tor MSHA
194 operon (Figure 2b). This suggests that, similar to other vibrios (15), the MSHA type IV
195 pilus plays an important role in resistance against the filamentous phage VALGΦ8. Note,
196 a search of all assembled genomes for CRISPR associated genes as well as for CRISPR
197 array like repetitive sequence patterns did not yield any results. All PCR-negative phage
198 resistant clones are from here onwards referred to as Φ-resistant mutants. The genomic
199 data also confirmed that clones with a positive PCR result (i.e., Φ-carrier) all contained
200 the respective phage genome, which existed episomally in all sequenced clones (Table
201 S2; Figures S3).

202 We found four PCR negative clones that were resistant to infections with ancestral
203 phages but did not acquire mutations within the MSHA operon or other loci that might
204 suggest a potential role in phage resistance. One explanation could be phenotypic
205 resistance, where phage adsorption to bacteria is strongly reduced (16).



206

207 **Figure 2** (A) Genetic loci on chromosome 1 under positive selection as indicated by parallel genomic
 208 evolution in populations exposed to phages: right: SIE hosts; middle: MSHA-mutants; left: zoom into
 209 MSHA-operon region from MSHA-mutants. Only loci which are not present in control populations are
 210 shown. Concentric circles correspond to one clone isolated from either the higher virulence VALGΦ_{8K04M5}
 211 (six inner circles, dark red) or the lower virulence VALGΦ_{8K04M1} phage (six outer circles, light red). Each
 212 coloured point corresponds to one mutation event on the respective clone. HP = hypothetical protein; HP3
 213 corresponds to locus tag K01M1_28150. For more detailed information on the underlying mutation see
 214 Table S1.

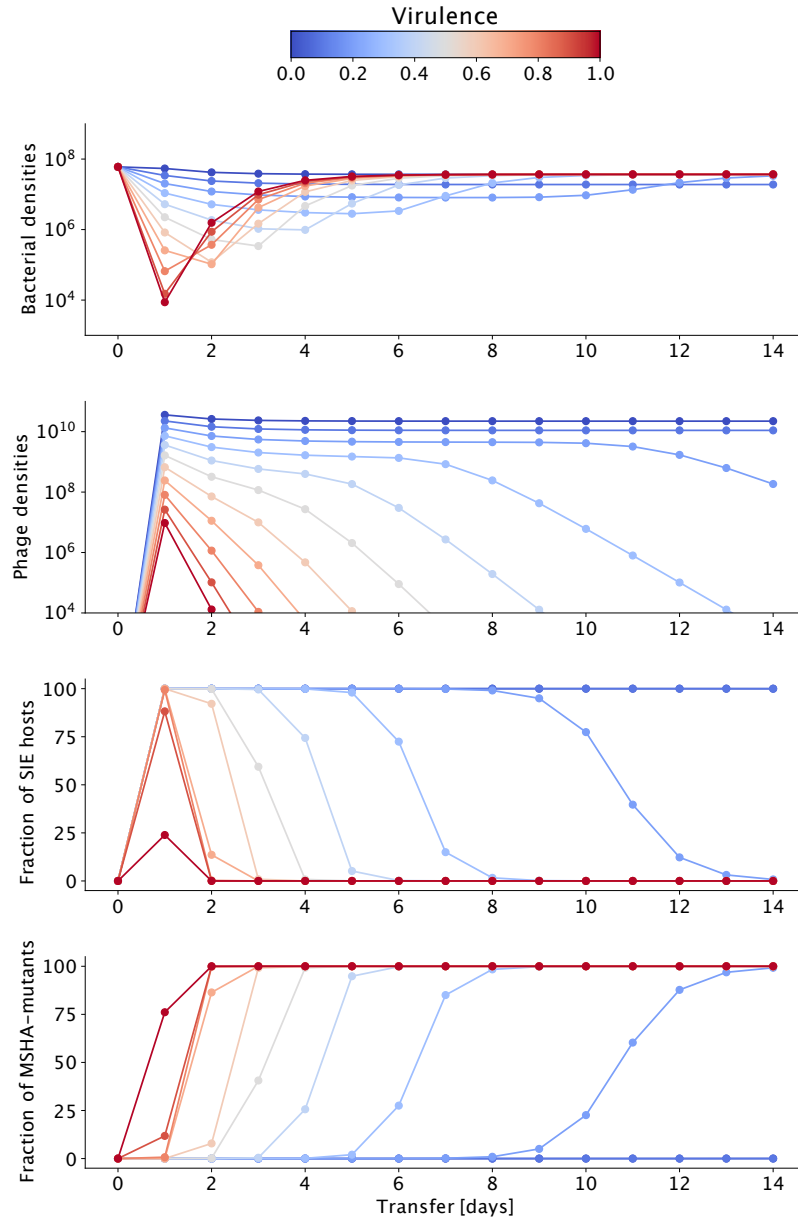
215 (B) Structure of the MSHA-operon and comparative genomics comprising MSHA-operons from *V.*
 216 *alginolyticus* FA2 (top), *V. alginolyticus* K01M1 (middle), and *V. cholerae* El Tor (bottom). Similarity
 217 between regions is indicated by dark grey blocks, genes with detected mutations are marked in orange,
 218 detected mutations are marked as arrows below *V. alginolyticus* K01M1.

219

220 Virulence determines the rate of resistance evolution in a mathematical model

221 To generalize our findings across a wider range of virulence levels we developed an
 222 experimentally parameterized mathematical model. As in the experiment, bacterial
 223 densities dropped by several orders of magnitude upon phage infection (Figure 3a). By

224 simulating the infection dynamics over a wider range over virulence levels, we found
225 that this drop occurred later and was less strong with decreasing virulence. While phage
226 densities (irrespective of virulence) peaked 24 hpi, phages persisted longer and at higher
227 levels when they were less virulent (Figure 3b). Similar to the experiment, the model
228 predicts that SIE immunity emerges rapidly within 24 hpi (Figure 3c) but will only reach
229 high levels if virulence is < 1 . To capture the displacement of SIE hosts by MSHA-
230 mutants we implemented a cost of reduced growth for SIE hosts which is directly linked
231 to virulence (due to intracellular production of viral particles (Figure 4c)), i.e., the higher
232 the virulence of the infecting phage, the lower the growth rate of the SIE host. MSHA-
233 mutants grew at the same rate as the non-resistant clones (Figure 4e). We found that
234 MSHA-mutants increased and replaced SIE hosts faster with increasing levels of
235 virulence (Figure 3 c,d). Our model shows that this replacement occurs across a wide
236 range of virulence levels, which we were not able to capture in the experiment. The
237 faster replacement of SIE hosts by MSHA-mutants at higher virulence levels is driven
238 by higher costs (i.e., reduced growth) of infection in SIE hosts, which increase
239 monotonically with increasing phage virulence. Overall, our simulations predict that
240 selection for resistance increases with virulence and that this is directly related to the
241 costs of SIE, and thus resistance is more likely to evolve against higher virulence
242 infections. This further suggests that to avoid extinction and enable long-term
243 persistence in bacterial populations, filamentous phages should evolve towards lower
244 virulence, reducing the cost of infection for SIE hosts and thus limiting selection for
245 resistance.



246

247 **Figure 3:** Results of model simulations of 14 transfers for (A) Bacteria in CFU/ml, (B) Phages in PFU/ml,
248 (C) SIE hosts, and (D) MSHA-mutants depending on phage virulence (colour coded from blue: no
249 virulence to red: high virulence).

250

251

252 **Relative fitness of resistant mutants increases with phage virulence**

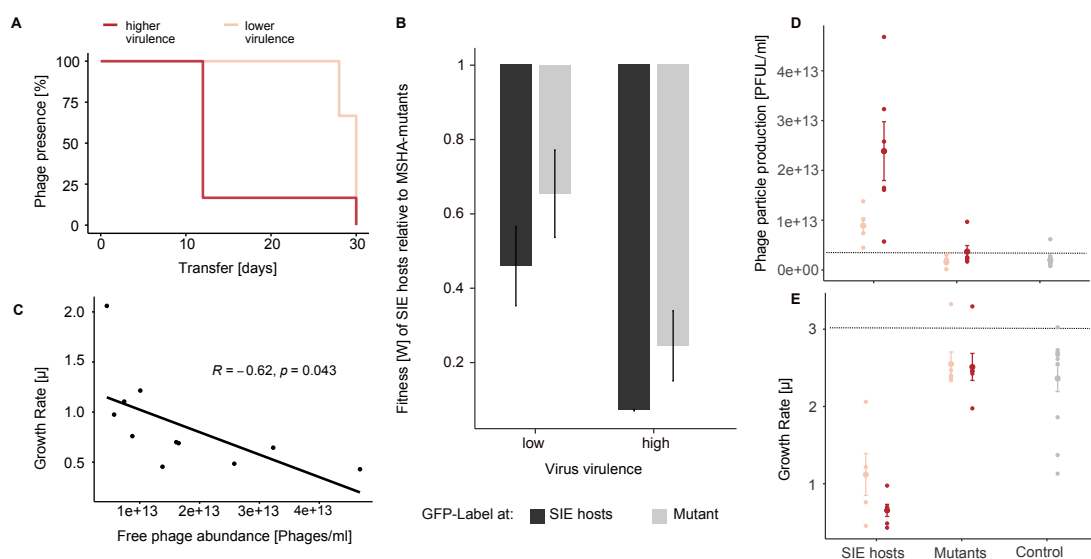
253 To directly test our model predictions, that the fitness benefit of resistance relative to

254 SIE immunity increases with increasing phage virulence, we performed a pairwise

255 competition experiment, in which we quantified the relative fitness of MSHA-resistant

256 mutants against SIE hosts (Figure 4b). The fitness benefit of the resistance mutation was

257 higher against bacteria carrying the higher virulence phage compared to bacteria carrying
 258 the lower virulence phage (significant treatment term in linear model with treatment,
 259 GFP-label and the interaction thereof as fixed factors: $F_{1,8}=18.63$, $p=0.003$, Table S3).
 260 These fitness data are consistent with the more rapid decline of VALGΦ8_{K04M5}-carriers
 261 than VALGΦ8_{K04M1}-carriers observed in the selection experiment and consistent with
 262 model predictions suggest stronger selection for resistance when exposed to a higher
 263 virulence phage. This explains the dynamics of the SIE hosts in the selection experiment,
 264 which went to extinction in five out of six populations exposed to the higher virulence
 265 phage 12 days post infection but were able to persist until the end of the experiment (i.e.,
 266 transfer 30), albeit at very low frequencies, in five out of six populations exposed to the
 267 lower virulence phage.
 268



269

270 **Figure 4 Phage prevalence (a) and fitness effects of evolved phage resistance versus immunity (b-**
 271 **e):** (a) Phage prevalence for each co-evolving population in the presence of higher virulence phage
 272 VALGΦ8_{K04M5} (dark red) or the lower virulence phage VALGΦ8_{K04M1} (light red) over 30 transfers. (b)
 273 Darwinian fitness of SIE hosts relative to MSHA-mutants. A value of one corresponds to equal fitness.
 274 To account for potential costs associated with the GFP protein, competitions were performed where either
 275 the SIE hosts or the MSHA-mutants were labelled ($n=3$). (c) Correlation between bacterial growth rate
 276 [μ] and production of free phages measured as PFU/ml per clone. (d) Phage particle production [PFU/ml]
 277 and (e) Growth rate μ : both measured after 24 hours of bacterial growth for SIE hosts, MSHA-mutants,
 278 clones from the control populations (grey), and the ancestral K01M1 strain (horizontal line). Clones
 279 exposed to lower virulent VALGΦ8_{K04M1} are shown in light red, clones exposed to higher virulent

280 VALGΦ_{8K04M5} in dark red. Phages from the ancestral K01M1, from MSHA-mutants and the control
281 clones stem from an ancestral filamentous *Vibrio* phage VALGΦ6 integrated on chromosome 2 of
282 K01M1 (Table 1). Shown are means ± SEM, n=24.
283
284

285 Bacterial population densities during the selection experiment were negatively
286 correlated with the number of SIE hosts per population (Pearson's correlation without
287 zero inflation Φ-K04M1: $r=0.69$, $t_{21}=-4.38$, $p<0.001$, Φ-K04M5: $r=0.92$, $t_7=-6.29$,
288 $p<0.001$; Figure S4). This implies that, even though the majority of the clones in the
289 populations were protected from further infection, bacterial populations were unable to
290 recover as long as the dominating mechanism of defence was SIE immunity,
291 presumably due to virulence, resulting from the strong reduction in bacterial growth
292 rate. To test this, we quantified differences in phage production and tested if phage
293 production impaired bacterial growth in evolved clones. VALGΦ_{8K04M5}-carriers
294 produced approximately 3.5 times more phage particles than VALGΦ_{8K04M1}-carriers
295 (VALGΦ_{8K04M5}: mean = 2.39×10^{13} PFU/ml ± 1.44×10^{13} , VALGΦ_{8K04M1}: mean =
296 8.92×10^{12} PFU/ml ± 3.43×10^{12} , Figure 4d), and phage production significantly impaired
297 bacterial growth (significant negative correlation between the amount of produced
298 phages and bacterial growth rate, Figure 4c). Direct comparisons of growth rates among
299 evolved clones showed that SIE hosts also grew slower than Φ-resistant mutants
300 (VALGΦ_{8K04M5}: paired t -test: $t_{6,93}=-9.69$, $p<0.001$; VALGΦ_{8K04M1}: paired t -test: $t_{6,5}=-$
301 4.58 , $p=0.003$, Figure 4e). Together, these data suggest that SIE buys time, offering
302 protection against subsequent infection, but at the cost of suffering the virulence of
303 being infected. As in the model, where we predicted that the costs of SIE increase
304 monotonically with phage virulence, SIE is eventually replaced by resistance, which
305 happens faster with increasing levels of virulence, where the fitness benefits of
306 resistance are greater. Ultimately dominance of host populations by resistant genotypes

307 resulted in faster extinction of higher virulence viruses, which were unable to overcome
308 evolved host resistance.

309

310 **Resistance leads to loss of motility**

311 Many structures on the bacterial cell surface that serve as receptors for phages are
312 multifunctional and phage resistance evolution through surface receptor modifications
313 can come with secondary costs, for a review, see (17). In the case of bacterial
314 appendages, such as flagella or pili, modifications often result in reduced motility
315 and/or virulence during eukaryotic infections (18). We thus tested whether the observed
316 mutations in the MSHA-pilus genes impair bacterial motility and observed reduced
317 swimming motility of mutants compared to ancestral strains (Video Supplementary
318 material). Since motility is an important fitness factor in the natural environment (18)
319 we predict that the replacement of SIE by non-motile MSHA-mutants is constrained to
320 laboratory environments, where such antagonistic pleiotropic costs of surface receptor
321 modifications are lower than the costs of SIE. Selective pressures occurring in the
322 natural environment, such as resource competition in eukaryotic hosts, might reverse
323 this effect and explain why filamentous phages, including high virulent versions of
324 VALGΦ8 persist in environmental isolates (19).

325

326 **Concluding remarks**

327 Filamentous phages are very common features of bacterial genomes (20), including
328 those of environmental *Vibrio* strains closely related to our model strain K01M1, of which
329 more than 50% are infected with the phage VALGΦ8 (19). While incorporating
330 filamentous phage genomes into their own genome provides bacteria with immunity to
331 future infection—through SIE immunity mediated by phage-encoded genes—we show

332 that this comes at a fitness cost that scales positively with the virulence of the phage.
333 Higher phage virulence selects for the more rapid replacement of SIE immunity with
334 resistance, causing phage extinction (Figure 4a). Thus, our data suggest, that to be able to
335 establish long-term chronic infections, filamentous phages must either evolve very low
336 levels of virulence (21), such that the resulting cost of virulence is outweighed by the cost
337 of resistance mutations, or they must contribute positively to bacterial fitness by providing
338 beneficial ecological functions (22). Those benefits may derive either from phage-
339 encoded gene functions (e.g., toxins) (23-25), or from properties of the phage particles
340 themselves (e.g., forming the biofilm extracellular-matrix (26), or acting as decoys for
341 the vertebrate immune response (27)). Phage-mediated fitness benefits are often
342 environmentally dependent (24, 28-30) and the prevalence of filamentous phages in
343 bacterial genomes is higher in those isolated from eukaryotic infections (where
344 filamentous phages often encode important enterotoxins) than those isolated from natural
345 environments (11). Even though we have not yet identified its actual benefit, the high
346 prevalence of VALGΦ8 in natural *V. alginolyticus* isolates (19) suggests that this phage
347 provides a selective advantage outside the laboratory in its natural environment, i.e., the
348 pipefish. Conversely, however, bacterial genomes are graveyards of defective prophages
349 (31), including filamentous phages (32), suggesting that decay, rather than a peaceful
350 coexistence, may be a common outcome for phages integrated into bacterial genomes.
351 Ultimately, their level of virulence will dictate the fate of filamentous phages: Whereas
352 lower virulence variants may enter into stable co-existence, higher virulence variants will
353 be more prone to resistance-driven extinction and mutational decay if they do not provide
354 a selective advantage.

355 MATERIAL AND METHODS

356 Experiments were conducted using the *Vibrio alginolyticus* strain K01M1 (33).
357 K01M1 contains one integrated filamentous *Vibrio* phage VALGΦ6 (later called:
358 resident K01M1Φ-phage throughout the manuscript), which replicates at a very low
359 frequency (19). Compared to other, closely related *V. alginolyticus* strains, K01M1 is
360 highly susceptible to infections by filamentous phages (14). For the selection experiment
361 we used two different isogenic versions of the filamentous *Vibrio* phage VALGΦ8:
362 VALGΦ8_{K04M1} (lower virulence) and VALGΦ8_{K04M5} (higher virulence; Table 1, for
363 similarity between phages see Supplementary information and Figure S1), which have
364 been isolated from two different hosts (*V. alginolyticus* K04M1 and *V. alginolyticus*
365 K04M5). While both phages have been shown to significantly reduce the growth of
366 K01M1 (14, 34), infections with the higher virulence VALGΦ8_{K04M5} impose a
367 significantly stronger reduction in bacterial growth than infections with the low virulence
368 phage VALGΦ8_{K04M1}. All experiments were carried out in liquid medium (Medium101:
369 0.5% (w/v) peptone, 0.3% (w/v) meat extract, 3.0% (w/v) NaCl in MilliQ water) at 25° C
370 in 30-ml microcosms containing 6 ml of medium with constant shaking at 180 rpm.

371

372 **Table 1** Bacteria and phages (including NCBI accession numbers) used in the present study.

Isolate	Accession Number(s)	Phages	Role in evolution experiment
<i>V. alginolyticus</i> K01M1	CP017889.1 CP017890.1	<i>Vibrio</i> phage VALGΦ6	Host strain during evolution experiment
<i>V. alginolyticus</i> K04M1	CP017891.1 CP017892.1	<i>Vibrio</i> phage VALGΦ6 <i>Vibrio</i> phage VALGΦ8	Donor of the episomal, low virulence phage
<i>V. alginolyticus</i> K04M5	CP017899.1 CP017900.1	<i>Vibrio</i> phage VALGΦ6 <i>Vibrio</i> phage VALGΦ8	Donor of the integrative, high virulence phage
<i>Vibrio</i> phage VALGΦ6	MN690600		Resident phage in ancestral K01M1
<i>Vibrio</i> phage VALGΦ8	MN719123		Phage used in selection experiment

373

374

375 (a) Selection experiment

376 Six replicate populations were founded for each of three treatments from independent
377 clones of K01M1. Treatments comprised (a) the higher virulence VALGΦ_{8K04M1}, (b) the
378 lower virulence VALGΦ_{8K04M5}, or (c) no phage as control. Each population was
379 established from 60 μl of an independent overnight culture (5×10⁸ CFU/ml). At the
380 beginning of the experiment, we inoculated phage-containing treatments with 300 μl of a
381 5×10¹⁰ PFU/ml stock solution. Populations were propagated by transferring 0.1% to fresh
382 medium every 24 hours for a total of 30 transfers. On transfer T0, T1, T2 followed by
383 every other transfer, phage and bacterial densities were determined, as described below
384 and whole population samples were frozen at -80° C at a final concentration of 33%
385 glycerol. In addition, on transfer T0, T1, T2, T6, followed by every sixth transfer 24 single
386 colonies were isolated at random from each population and stored at -80° C. These
387 colonies were later used during follow-up assays, as described below. Two populations
388 from the control treatment tested positive for virus infection, indicating contamination,
389 were excluded from later assays.

390

391 (b) Bacterial and phage densities

392 *Bacterial densities:* bacterial densities were determined by plating out 100 μl of a
393 dilution series ranging from 10⁻⁵ to 10⁻⁷ on *Vibrio* selective Thiosulfate Citrate Bile
394 Sucrose Agar (TCBS) plates (Sigma Aldrich). Plates were incubated over night at 25° C
395 and the total amount of colonies was counted the following day.

396 *Phage densities:* quantification of filamentous phages by standard spot assays is often
397 not possible (Rakonjac 2011). Instead of typical lytic plaques we mostly observed opaque
398 zonas of reduced growth. Thus, we used spectrometry to quantify phage prevalence
399 (<http://www.abdesignlabs.com/technical-resources/bacteriophage-spectrophotometry>),

400 which uses the constant relationship between the length of viral DNA and the amount of
401 the major coat protein VIII of filamentous phages, which, together, are the main
402 contributors of the absorption spectrum in the UV range. The amount of phage particles
403 per ml can be calculated according to the following formula:

$$404 \quad \text{phages/ml} = \frac{(\text{OD}_{269} - \text{OD}_{320}) * 6e16}{\text{bp}},$$

405 where OD₂₆₉ and OD₃₂₀ stand for optical density at 269 and 320 nm and bp stands for
406 number of base pairs per phage.

407 The method is based on small-scale precipitation of phages by single PEG-
408 precipitation. After centrifuging 1500 μ l of the phage containing overnight culture at
409 13,000 \times g for 2 min, 1200 μ l of the supernatant was mixed with 300 μ l PEG/NaCl 5 \times and
410 incubated on ice for 30 min. Afterwards phage particles were pelleted by two rounds of
411 centrifugation at 13,000 \times g for 2 min, resuspended in 120 μ l TBS 1 \times and incubated on
412 ice. After one hour the suspension was cleaned by centrifugation at 13,000 \times g for 1 min
413 and absorbance was measured at 269 and 320 nm.

414 Quantification of filamentous phages using spectrometry is likely to be erroneous if
415 viral load is low. Therefore, we additionally quantified phage prevalence/ phage
416 extinction in each of the populations on every second transfer day by standard spot assays
417 with a serial dilution (up to 10⁻⁶) on the ancestral host (for details see (14)) and measured
418 until which dilution the typical opaque zones of reduced bacterial growth were visible.

419

420 (c) Measuring phage-defence

421 We quantified the bacteria could not get infected by the respective ancestral phage
422 by determining the reduction in bacterial growth rate (RBG) imposed by the phage,
423 adapted from (35) with some modifications according to (36). Twenty-four random
424 colonies from each population from transfer T0, T1, T2, T6, T12, T18, T24, and T30 were

425 introduced into 96-well microtiter plates containing Medium101 at a concentration of
426 5×10^6 cells/ml and inoculated with $\sim 2.5 \times 10^6$ PFU/ml of the respective ancestral phage
427 used for the selection experiment or without phage (control). Absorbance at 600 nm was
428 measured using an automated plate reader (TECAN infinite M200) at T0 and again after
429 20 hours of static incubation at 25°C. The reduction in bacterial absorbance ‘RBG’ was
430 calculated according to the following formula:

$$431 \quad \text{RBG} = \frac{\text{OD}_{600}(t=20) - \text{OD}_{600}(t=0)_{\text{[Phage]}}}{\text{OD}_{600}(t=20) - \text{OD}_{600}(t=0)_{\text{[Control]}}}$$

432 where OD stands for optical density at 600nm.

433

434 (d) Frequency of prophage carriage

435 On transfer T0, T1, T2, T6 followed by every sixth transfer we measured the
436 frequency of phage carriage of 24 random clones per population using standard PCR.
437 Primers (VALGΦ8_Forward TGGAAGTGCCAAGGTTTGGT, VALGΦ8_Revers
438 GAAGACCAGGTGGCGGTAAA) that specifically target the *Vibrio* phage VALGΦ8
439 have been designed using NCBI Primer-BLAST webpage
440 (<http://www.ncbi.nlm.nih.gov/tools/primer-blast/>). Glycerol stocks were inoculated
441 overnight (25°C, 180 rpm) in Medium101 and subsequently diluted (1:10) in HPLC
442 purified H₂O and frozen at -80° C. One μl of this suspension was used as DNA template
443 in the PCR assay. Reaction comprised 1 μl Dream Tag Buffer, 0.1 μl Dream Tag DNA
444 polymerase (Thermo Scientific, USA), 4.9 μl H₂O, 1 μl dNTPs [5 mM] and 1 μl of each
445 primer [50 μM]. The amplification program used consisted of: (i) 3 min at 95° C, (ii) 35
446 cycles of 45 sec at 95° C, 30 sec at 63° C, 45 sec at 72° C, (iii) 7 min at 72° C. Afterwards,
447 5 μl of each reaction was mixed with 2 μl loading dye (10 \times) and loaded onto a 1.2%
448 agarose gel dissolved in 1 \times TAE gel buffer. GeneRuler Express DNA-ladder was used as
449 size marker. Agarose gels were run 15 min at 70 V in 0.5 \times TAE running buffer and

450 subsequently stained with ethidium bromide for 10 min. DNA was visualized using UV
451 light and documentation took place using Intas Gel iX20 Imager. Phage presence was
452 recorded positive if a PCR product of 1209 bp was visible.

453 For all subsequent assays, we randomly picked one immune clone with a positive
454 PCR product (later called: Φ -carrier) and one resistant clone with a negative PCR product
455 (later called: Φ -resistant mutant) from each phage-evolved population as well as two
456 randomly selected non-resistant clones from the control populations.

457

458 (e) Competition experiments

459 To determine differences in fitness between both resistance forms, we measured the
460 competitive fitness of three randomly selected Φ -carrier relative to three randomly
461 selected Φ -resistant mutants from each treatment. Each competition culture was done in
462 triplicates as described in (37). In brief, overnight cultures of both competing strains (of
463 which one was labelled with a GFP-marker) were mixed 1:1 and 60 μ l of this mixture
464 was inoculated to 6 ml Medium 101 to initiate each competitive culture. After 24 hours,
465 fitness was estimated by means of flow cytometry (FACS-Calibur^m Becton & Dickinson,
466 Heidelberg, GER), where absolute fluorescent cells and non-fluorescent cells were
467 calculated. Competitive fitness was estimated as the ratio in Malthusian parameters (38):

468

$$469 \quad W = \ln(\text{abundance}_{t=24} / \text{abundance}_{t=0})_{\text{competitor1}} / \ln(\text{abundance}_{t=24} / \text{abundance}_{t=0})_{\text{competitor2}}$$

470

471 (f) Bacterial growth rate and phage production

472 To determine fitness parameters that could explain observed differences in competitive
473 fitness we additionally quantified bacterial growth rate (μ) by means of 24-hour growth
474 curves and phage production using PEG precipitation (as described in (c)) of the same

475 clones used for the competition assays (i.e., one Φ -carrier and one Φ -resistant mutant
476 from each phage-treated population and two random phage-susceptible clones from the
477 control populations plus ancestors).

478

479 (g) Motility

480 Motility was visualized on mid-exponential growth cultures using a light
481 microscope and swimming was captured for 50s.

482

483 (h) Whole genome sequencing

484 We used a combination of long- and short read sequencing to obtain complete
485 genomes of the same clones from the assays above, i.e., one Φ -carrier and one Φ -resistant
486 mutant from each phage-treated population and one random phage-susceptible clone from
487 each control population, which corresponds to six independently evolved clones per
488 treatment and resistance form. Clones were taken from timepoint 2, because phage-
489 carriers disappeared quickly from the populations and we were thus not able to pick one
490 mutant and one Φ -carrier from the same timepoint and population later than timepoint
491 two. High molecular weight DNA was extracted from cell pellets of overnight cultures
492 following the protocol for gram negative bacteria from the DNeasy Blood & Tissue Kit
493 (Qiagen, Hilden, Germany). Long-read sequencing was performed at the Norwegian
494 Sequencing Centre according to the following protocol: the library was prepared using
495 Pacific Bioscience protocol for SMRTbell™ Libraries using PacBio® Barcoded Adapters
496 for Multiplex SMRT® Sequencing. To do so, DNA was fragmented into 10kb fragments
497 using g-tubes (Covaris). Samples were pooled during library preparation aiming for
498 equimolar pooling and library size was selected using Ampure beads. The library was
499 sequenced on a PacBio Sequel instrument using Sequel Polymerase v3.9, SMRT cells v3

500 LR and Sequencing chemistry v3.0. Loading was performed by diffusion. Two SMRT
501 cells were sequenced (movie time: 600min, pre-extension time: 240 min). Reads were
502 demultiplexed using Barcoding pipeline on SMRT Link (v6.0.0.47841, SMRT Link
503 Analysis Services and GUI v6.0.0.47836) with 40 as a minimum barcode score.

504 For short read sequencing concentration and purity of the isolated DNA was first
505 checked with a Nanodrop ND-1000 (PeqLab Erlangen, Germany) and exact concentration
506 was determined using the Qubit® dsDNA HS Assay Kit as recommended by the
507 manufacturer (Life Technologies GmbH, Darmstadt, Germany). Illumina shotgun
508 libraries were prepared using the Nextera XT DNA Sample Preparation Kit. To assess
509 quality and size of the libraries, samples were run on an Agilent Bioanalyzer 2100 using
510 an Agilent High Sensitivity DNA Kit as recommended by the manufacturer (Agilent
511 Technologies, Waldbronn, Germany). Concentration of the libraries were determined
512 using the Qubit® dsDNA HS Assay Kit as recommended by the manufacturer (Life
513 Technologies GmbH, Darmstadt, Germany). Sequencing was performed on a MiSeq
514 system with the reagent kit v3 with 600 cycles (Illumina, San Diego, CA, USA) as
515 recommended by the manufacturer and resulted in a minimum average coverage of 88×
516 per strain (coverage range was from 88× to 157×). The reads were quality controlled using
517 the program FastQC Version 0.11.5. All illumina reads that passed the FastQC filtering
518 were used for hybrid assemblies as well as for single nucleotide variation analysis.

519 Genome assemblies were performed in two different ways: (i) long-read data was
520 generated for all replicates where the presence of the infecting phage was confirmed by
521 PCR. The Assemblies were performed as hybrid assemblies using short-read and long
522 read data in a short-read first approach. In brief: An initial assembly was performed with
523 short-read only using spades (v3.13.0) as provided within Unicycler (39). The resulting
524 contigs were co-assembled with long-read data using miniasm (v0.2-r168) (40) and

525 curated using the racon software (41). This step resulted in complete closed replicons. All
526 long reads were mapped and integrated into the contigs. All replicons were polished using
527 Pilon (v1.22) to clear any small-scale assembly errors (42). Finally, all replicons were
528 rearranged according to the origin of replication. (ii) the assembly for the ancestral
529 K01M1 strain, as has been described in (14) was performed following the Hierarchical
530 Genome Assembly Process (HGAP3) protocol, developed for Pacific Biosciences Single
531 Molecule Real-Time (SMRT) sequencing data (43). HGAP is available for use within
532 PacBio's Secondary Analysis Software SMRTPortal. Methodically, the longest subreads
533 of a single SMRT Cell (usually 25x genome coverage, e.g., 25 x 5 Mbp = 125 Mbp) are
534 being chosen to be error-corrected with "shorter" long reads in a process named
535 preassembly. Hereby, a length cut-off is computed automatically separating the "longer"
536 reads (for genome assembly) and the "shorter" reads (for error-correction). The level of
537 error-correction is being estimated with a per-read accuracy of 99%. Finally, error-
538 corrected long read data is being assembled with Celera Assembler (v7.0) (44).

539

540 (i) SNV analysis and reconstruction of infecting phages

541 All short-read sequences were mapped on a high quality closed reference genome of
542 *Vibrio alginolyticus* Strain K01M1 (14) using Bowtie2 (45). Single nucleotide variation
543 (SNV) analysis was done using the Breseq pipeline as described in (46). Whole genome
544 alignments have been calculated using the MAUVE aligner (47). Presence of infecting
545 phage genomes were confirmed by assembling NGS-reads that did not map on the
546 K01M1 genome in a bowtie2 mapping using Spades (39). The resulting contigs were
547 annotated based on the review of Mai-Prochnow on filamentous phages (11). The
548 genomes of the evolved phages were compared to the infecting phage genomes *Vibrio*
549 phage VALGΦ8 as well as to the genome of the resident prophage *Vibrio* phage

550 VALGΦ6 from the challenged strain K01M1 using BLAST and Easyfig 2.1 (48).

551

552 (j) Statistical analysis

553 All statistics were performed in the R 4.0.4 statistical environment (49). For all
554 analysis aimed to compare the two different phage treatments to one another, control
555 populations (i.e., those that evolved without phages) were excluded. When comparing
556 temporal dynamics between phage-treatments, we excluded the starting time-point T₀,
557 because these measurements were taken before phages were added to the populations.

558

559 *Bacteria and phage dynamics*

560 Bacterial and phage densities were analysed over time using a generalized least
561 squares model to control for autocorrelation of residuals over time using the gls function
562 (package nlme) with phage treatment, transfer as categorical variable as well as their
563 interaction as fixed effect.

564 We considered phages to be prevalent in the population if opaque zones of reduced
565 growth were visible during standard spot assays. Phage prevalence was subsequently
566 quantified by a serial dilution, which were assigned with invers values (i.e., if reduced
567 growth zones were visible up to dilution of 10⁻⁶ we assigned to it a value of 7, whereas if
568 they were only visible on an undiluted spot, we assigned to it a value of 1, if no zone of
569 reduced growth was visible it was scored as 0). Phage extinction events across phage-
570 treatments were analysed using a log-rank test.

571

572 *Measuring phage defence and prevalence*

573 We observed a bimodal histogram on all RBG values with a local minimum at RBG
574 = 0.82 (Figure S2). Thus, we considered an infection as positive if RBG < 0.82. The

575 proportion of clones per population that could not get infected by the ancestral phage as
576 well as the proportion of clones that tested positive for PCR (targeting the VALGΦ8)
577 were analysed using a generalized linear model with a binomial error distribution using
578 the glm function (package lme4) with phage treatment, transfer and their interaction as
579 fixed effect.

580

581 *Fitness effects*

582 We determined differences in relative fitness between MSHA-mutants and SIE hosts
583 using a linear model with resistance mechanisms and GFP-label and the interaction
584 thereof as fixed effects. Maximum growth rates (μ) were estimated for each strain by
585 fitting generalized logistic models to individual growth curves using the open-source
586 software package Curveball (<https://github.com/yoavram/curveball>) (50) in python. To
587 determine differences in the amount of free phages and in growth rates produced
588 between ancestral strains and evolved strains and between both resistance forms, we
589 used Welch's pairwise *t*-tests with sequential Bonferroni correction. We further
590 performed a Pearson's correlation analysis to determine whether phage production
591 impacted bacterial growth rates.

592

593 (k) Mathematical model

594 We modelled the dynamics of the non-resistant evolved clones (with density B),
595 resistant SIE hosts (I), resistant MSHA-mutants (R), and SIE hosts that have also
596 acquired the MSHA mutation (IR), as well as the phage population (V) in batch cultures
597 by the following system of differential equations:

598
$$\frac{dB}{dt} = (1 - m)g(B_{total})B - \phi BV$$

599
$$\frac{dI}{dt} = (1 - m)(1 - v)g(B_{total})I + \phi BV$$

600
$$\frac{dR}{dt} = (R + mB)g(B_{total})$$

601
$$\frac{dIR}{dt} = ((1 - v)IR + mI)g(B_{total})$$

602
$$\frac{dV}{dt} = \beta(I + IR) - dV$$

603

604 Bacterial growth was modelled by generalized logistic growth of the form

605 $g(B_{total}) = r \left(1 - \left(\frac{B_{total}}{K}\right)^w\right)$. Here r is the maximum growth rate (mgr) of the non-

606 resistant evolved bacteria, K is the carrying capacity of the batch culture and $B_{total} =$

607 $B + I + R + IR$ is the total density of all bacterial types. The curvature parameter w

608 determines whether maximum growth is attained at an early point in the growth phase

609 ($w < 1$) or at a late point ($w > 1$). We assume that SIE hosts (I and IR) suffer a growth

610 rate reduction relative to the non-resistant evolved bacteria due to virulence caused by

611 intra-cellular production of virus particles, here represented by the virulence factor $v <=$

612 1. A completely avirulent virus would have $v=0$, and maximum virulence $v=1$

613 corresponds to growth arrest of the bacterial cell.

614 Viruses (V) infect non-resistant evolved bacteria (B) following a mass action law

615 with adsorption rate (ϕ), reflecting that increasing densities of either bacteria or viruses

616 lead to higher encounter rates and thus more infections. Infection of a bacterial cell

617 transforms cells into a resistant Φ -carrier (I), which actively produces new viral particles

618 (V) with phage production rate (β). Additionally, both non-resistant evolved bacteria (B)

619 and SIE hosts (I) can acquire complete resistance (R & IR) through mutations within the

620 MSHA type IV pilus operon. We assume that MSHA-mutants have the same growth

621 rate as the non-resistant evolved bacteria.

622 All bacterial types grow until the carrying capacity (K) is reached, but bacteria-virus
623 interactions continue to occur as long as there are sensitive bacteria and viruses left.
624 After a certain time t_{max} a portion (here 1/1000th) of the entire community is transferred
625 to fresh medium and the process restarts.

626

627 **Table 2** Parameter values of mathematical model and their biological meaning

Parameter	Biological meaning	Value
r	Maximum growth rate (mgr) of ancestor B	2.5 (h^{-1})
K	Carrying capacity of bacteria	10^9 cells/ml
w	Curvature parameter	0.02
v	Virulence	variable
ϕ	Phage adsorption rate	10^{-8} (h^{-1})
β	Phage production rate	50 (phages/cell h^{-1})
d	Phage decay rate	0.01 (h^{-1})
m	Mutation rate	10^{-8}

628

629 **Acknowledgements:** We thank Pratheeba Pandiaraj, Katja Trübenbach, Veronique
630 Merten, Silke-Mareike Merten and Kim-Sara Wagner for their support in the laboratory.

631

632 **Funding:** This project received funding from three grants from the DFG [WE 5822/ 1-
633 1], [WE 5822/ 1-2], and [OR 4628/ 4-2] within the priority programme SPP1819 given
634 to CCW and OR and a DFG grant within the Cluster of Excellence 80 “The Future Ocean”
635 given to CCW.

636

637 **Data availability:** All experimental data have been deposited on dryad (a link will be
638 provided upon acceptance of the manuscript). Genomic data is available at NCBI
639 (accession number will be provided upon acceptance of the manuscript), and in the
640 supplemental data file Table S1 and S2.

641

642 **References**

643

644 1. F. Fenner, I. D. Marshall, A comparison of the virulence for European rabbits
645 (Oryctolagus cuniculus) of strains of myxoma virus recovered in the field in
646 Australia, Europe and America. *The Journal of hygiene* **55**, 149-191 (1957).

647 2. S. R. Weiss, J. L. Leibowitz, Chapter 4 - Coronavirus Pathogenesis. *Advances*
648 *in Virus Research* **81**, 85-164 (2011).

649 3. S. L. Messenger, I. J. Molineux, J. J. Bull, Virulence evolution in a virus obeys
650 a trade-off. *Proceedings. Biological sciences* **266**, 397-404 (1999).

651 4. P. E. Turner, V. S. Cooper, R. E. Lenski, Tradeoff between Horizontal and
652 Vertical Modes of Transmission in Bacterial Plasmids. *Evolution* **52**, 315-329
653 (1998).

654 5. J. J. Bull, I. J. Molineux, W. R. Rice, Selection of Benevolence in a Host-Parasite
655 System. *Evolution* **45**, 875-882 (1991).

656 6. E. A. Herre, Population structure and the evolution of virulence in nematode
657 parasites of fig wasps. *Science* **259**, 1442-1445 (1993).

658 7. D. Ebert, Virulence and Local Adaptation of a Horizontally Transmitted
659 Parasite. *Science* **265**, 1084-1086 (1994).

660 8. M. Boots, Y. Haraguchi, The Evolution of Costly Resistance in Host-Parasite
661 Systems. *Am Nat* **153**, 359-370 (1999).

662 9. O. Restif, J. C. Koella, Shared control of epidemiological traits in a
663 coevolutionary model of host-parasite interactions. *Am Nat* **161**, 827-836 (2003).

664 10. M. van Baalen, Coevolution of recovery ability and virulence. *Proceedings.*
665 *Biological sciences* **265**, 317-325 (1998).

666 11. A. Mai-Prochnow *et al.*, 'Big things in small packages: the genetics of
667 filamentous phage and effects on fitness of their host'. *Fems Microbiol Rev*
668 10.1093/femsre/fuu007 (2015).

669 12. J. Bondy-Denomy, A. R. Davidson, When a Virus is not a Parasite: The
670 Beneficial Effects of Prophages on Bacterial Fitness. *J Microbiol* **52**, 235-242
671 (2014).

672 13. D. Refardt, Within-host competition determines reproductive success of
673 temperate bacteriophages. *Isme J* **5**, 1451-1460 (2011).

- 674 14. C. C. Wendling *et al.*, Tripartite species interaction: eukaryotic hosts suffer more
675 from phage susceptible than from phage resistant bacteria. *BMC Evol Biol* **17**
676 (2017).
- 677 15. E. A. Jouravleva *et al.*, The *Vibrio cholerae* mannose-sensitive hemagglutinin is
678 the receptor for a filamentous bacteriophage from *V. cholerae* O139. *Infect*
679 *Immun* **66**, 2535-2539 (1998).
- 680 16. J. J. Bull, C. S. Vegge, M. Schmerer, W. N. Chaudhry, B. R. Levin, Phenotypic
681 resistance and the dynamics of bacterial escape from phage control. *PLoS One*
682 **9**, e94690 (2014).
- 683 17. M. Leon, R. Bastias, Virulence reduction in bacteriophage resistant bacteria.
684 *Front Microbiol* **6**, 343 (2015).
- 685 18. T. Proft, E. N. Baker, Pili in Gram-negative and Gram-positive bacteria -
686 structure, assembly and their role in disease. *Cell Mol Life Sci* **66**, 613-635
687 (2009).
- 688 19. C. M. Chibani, R. Hertel, M. Hoppert, H. Liesegang, C. C. Wendling, Closely
689 Related *Vibrio alginolyticus* Strains Encode an Identical Repertoire of
690 Caudovirales-Like Regions and Filamentous Phages. *Viruses* **12** (2020).
- 691 20. S. Roux *et al.*, Cryptic inoviruses revealed as pervasive in bacteria and archaea
692 across Earth's biomes. *Nat Microbiol* **4**, 1895-1906 (2019).
- 693 21. T. J. Lerner, P. Model, The "steady state" of coliphage f1: DNA synthesis late in
694 infection. *Virology* **115**, 282-294 (1981).
- 695 22. I. D. Hay, T. Lithgow, Filamentous phages: masters of a microbial sharing
696 economy. *Embo Rep* **20** (2019).
- 697 23. M. K. Waldor, J. J. Mekalanos, Lysogenic conversion by a filamentous phage
698 encoding cholera toxin. *Science* **272**, 1910-1914 (1996).
- 699 24. M. D. Gonzalez, C. A. Lichtensteiger, R. Caughlan, E. R. Vimr, Conserved
700 filamentous prophage in *Escherichia coli* O18:K1:H7 and *Yersinia pestis* biovar
701 *orientalis*. *J Bacteriol* **184**, 6050-6055 (2002).
- 702 25. S. A. Rice *et al.*, The biofilm life cycle and virulence of *Pseudomonas aeruginosa*
703 are dependent on a filamentous prophage. *Isme J* **3**, 271-282 (2009).
- 704 26. P. R. Secor *et al.*, Filamentous Bacteriophage Promote Biofilm Assembly and
705 Function. *Cell Host Microbe* **18**, 549-559 (2015).

- 706 27. J. M. Sweere *et al.*, Bacteriophage trigger antiviral immunity and prevent
707 clearance of bacterial infection. *Science* **363**, 1416-+ (2019).
- 708 28. C. C. Wendling, D. Refardt, A. R. Hall, Fitness benefits to bacteria of carrying
709 prophages and prophage-encoded antibiotic-resistance genes peak in different
710 environments. *Evolution* 10.1111/evo.14153 (2020).
- 711 29. I. Chouikha, L. Charrier, S. Filali, A. Derbise, E. Carniel, Insights into the
712 infective properties of Ypf Phi, the *Yersinia pestis* filamentous phage. *Virology*
713 **407**, 43-52 (2010).
- 714 30. A. Derbise *et al.*, A horizontally acquired filamentous phage contributes to the
715 pathogenicity of the plague bacillus. *Mol Microbiol* **63**, 1145-1157 (2007).
- 716 31. L. M. Bobay, M. Touchon, E. P. C. Rocha, Pervasive domestication of defective
717 prophages by bacteria. *P Natl Acad Sci USA* **111**, 12127-12132 (2014).
- 718 32. B. M. Davis, K. E. Moyer, E. F. Boyd, M. K. Waldor, CTX prophages in
719 classical biotype *Vibrio cholerae*: functional phage genes but dysfunctional
720 phage genomes. *J Bacteriol* **182**, 6992-6998 (2000).
- 721 33. C. M. Chibani, O. Roth, H. Liesegang, C. C. Wendling, Genomic variation
722 among closely related *Vibrio alginolyticus* strains is located on mobile genetic
723 elements. *Bmc Genomics* **21**, 354 (2020).
- 724 34. C. C. Wendling, H. Goehlich, O. Roth, The structure of temperate phage-bacteria
725 infection networks changes with the phylogenetic distance of the host bacteria.
726 *Biol Lett* **14** (2018).
- 727 35. V. Poullain, S. Gandon, M. A. Brockhurst, A. Buckling, M. E. Hochberg, The
728 evolution of specificity in evolving and coevolving antagonistic interactions
729 between a bacteria and its phage. *Evolution* **62**, 1-11 (2008).
- 730 36. H. Goehlich, O. Roth, C. C. Wendling, Filamentous phages reduce bacterial
731 growth in low salinities. *Royal Society open science* **6**, 191669 (2019).
- 732 37. E. Harrison, D. Guymer, A. J. Spiers, S. Paterson, M. A. Brockhurst, Parallel
733 Compensatory Evolution Stabilizes Plasmids across the Parasitism-Mutualism
734 Continuum. *Curr Biol* **25**, 2034-2039 (2015).
- 735 38. R. E. Lenski, M. R. Rose, S. C. Simpson, S. C. Tadler, Long-Term Experimental
736 Evolution in *Escherichia-Coli* .1. Adaptation and Divergence during 2,000
737 Generations. *Am Nat* **138**, 1315-1341 (1991).
- 738 39. A. Bankevich *et al.*, SPAdes: a new genome assembly algorithm and its
739 applications to single-cell sequencing. *J Comput Biol* **19**, 455-477 (2012).

- 740 40. H. Li, Minimap and miniasm: fast mapping and de novo assembly for noisy long
741 sequences. *Bioinformatics* **32**, 2103-2110 (2016).
- 742 41. R. Vaser, I. Sovic, N. Nagarajan, M. Sikic, Fast and accurate de novo genome
743 assembly from long uncorrected reads. *Genome Res* **27**, 737-746 (2017).
- 744 42. B. J. Walker *et al.*, Pilon: an integrated tool for comprehensive microbial variant
745 detection and genome assembly improvement. *PLoS One* **9**, e112963 (2014).
- 746 43. C. S. Chin *et al.*, Nonhybrid, finished microbial genome assemblies from long-
747 read SMRT sequencing data. *Nat Methods* **10**, 563-569 (2013).
- 748 44. G. Denisov *et al.*, Consensus generation and variant detection by Celera
749 Assembler. *Bioinformatics* **24**, 1035-1040 (2008).
- 750 45. B. Langmead, S. L. Salzberg, Fast gapped-read alignment with Bowtie 2. *Nat*
751 *Methods* **9**, 357-359 (2012).
- 752 46. D. E. Deatherage, J. E. Barrick, Identification of mutations in laboratory-evolved
753 microbes from next-generation sequencing data using breseq. *Methods Mol Biol*
754 **1151**, 165-188 (2014).
- 755 47. A. E. Darling, B. Mau, N. T. Perna, progressiveMauve: multiple genome
756 alignment with gene gain, loss and rearrangement. *PLoS One* **5**, e11147 (2010).
- 757 48. M. J. Sullivan, N. K. Petty, S. A. Beatson, Easyfig: a genome comparison
758 visualizer. *Bioinformatics* **27**, 1009-1010 (2011).
- 759 49. R. D. C. Team, R: A language and environment for statistical computing. R
760 Foundation for Statistical Computing. *Vienna, Austria. ISBN 3-900051-07-0,*
761 *URL <http://www.R-project.org/>.* (2011).
762
- 763 50. Y. Ram *et al.*, Predicting microbial growth in a mixed culture from growth curve
764 data. *Proc Natl Acad Sci U S A* **116**, 14698-14707 (2019).